JOURNAL OF EXPERIMENTAL AND THEORETICAL PHYSICS, 2024, Vol. 165, No. 4, pp. 522–532

SOLIDS AND LIQUIDS

MODELING THE FORMATION PROCESSES OF STRUCTURE IN Ag–Au BIMETALLIC NANOCLUSTERS

© 2024 S. L. Gafner*, Yu. Ya. Gafner, L. V. Redel, Zh. V. Golovenko

Katanov Khakass State University,
655017, Abakan, Russia

**e-mail: sgafner@rambler.ru*

Received July 28, 2023
Revised November 14, 2023
Accepted November 15, 2023

Abstract. In the production of SERS substrates, two main approaches are used to form an array of plasmonic nanoparticles: photolithography and chemical methods, each having its advantages and disadvantages. Another possible method is thermal evaporation in vacuum, which was chosen for analysis through computer modeling. For this purpose, molecular dynamic simulation of crystallization processes of binary Ag–Au nanoparticles array was used, allowing smooth adjustment of the plasmon resonance wavelength. Three arrays of Ag–Au nanoparticles with diameter 2.0, 4.0 and 6.0 nm of various target compositions from $Ag_{90}Au_{10}$ to $Ag_{50}Au_{50}$ were created and subjected to cooling procedure from melt with different rates of thermal energy removal. During the modeling of Ag–Au nanoparticles internal structure formation, conclusions were drawn about the dependence of these processes on target composition, size, and level of thermal exposure. Based on the obtained patterns, adjustments to the technological process of creating SERS substrates using binary Ag–Au nanoparticles were proposed.

Keywords: *nanoclusters, silver, gold, crystallization, structure, computer modeling, tight-binding*

DOI: 10.31857/S004445102404e060

1. INTRODUCTION

Currently, metallic nanomaterials of various types are already widely used in numerous fields of science and technology due to their special catalytic, magnetic, optical, and mechanical properties in comparison to their corresponding bulk materials. Let's consider just one of their possible application areas, namely their use in nano-optics. Here, nanoparticles of certain metals, due to the phenomenon of localized surface plasmon resonance (LSPR), can serve as unique antennas for electromagnetic wave energy transmission [1, 2], which presents the broadest scope for their technical application [3]. Another well-known way of using plasmonic nanostructures is surface-enhanced Raman scattering (SERS) [1]. The sensitivity increase of SERS structures can be achieved by increasing the incident electromagnetic wave energy due to field enhancement near nanoparticle surfaces, also because of localized plasmon resonance. However, these behavioral features of metallic nanoparticles strongly depend on the nanomaterial synthesis method, as it determines their final shape, size, internal structure, composition, and chemical stability.

Let us further focus on the structure of nanoparticles obtained through various synthesis methods. It is assumed that monometallic nanoparticles have three main structural forms: decahedral (Dh), cuboctahedral (BCC, FCC, or HCP), and icosahedral (Ih). In an icosahedron, the main emphasis is on the formation of (111) planes, which leads to the lowest surface energy but implies significant internal deformation of the nanoparticle core. In the case of a cuboctahedron, there is no such core deformation, and the significantly larger surface energy of the particle is observed mainly due to the formation of (111) and (100) planes. The decahedron has moderate internal deformation and smaller facets also from planes (111) and (100), being essentially an intermediate form between the icosahedron and the structure characteristic of the bulk phase. Thus, in the case of monometallic nanoparticles, the following explicit

relationship between surface energies is observed γ: $\gamma(111) < \gamma(100) < \gamma(110)$.

The addition of a second metal to a nanoparticle leads to significant changes in its physicochemical properties, which is also reflected in changes in its morphology. Experimental and theoretical data demonstrate significant fluctuations in thermodynamics and structure formation processes of small nanoclusters even when only one impurity atom is added. Moreover, nanoalloys can exhibit a more diverse spectrum of internal structure, including irregular morphology (triangular, hexagonal, quasi-elongated plates, etc.) [4, 5]. It can also be of mixed or chemically phase-separated type [6], for example, representing a core-shell structure where the core of one atomic species is covered with a shell of the second chemical element [7, 8]. Janus-like particles can also be formed, where different metals of the alloy are separated in two halves of a single nanoparticle. Additionally, nanoparticles synthesized by physical methods, mainly through variations of gas phase condensation, often represent multiple non-crystalline structures. Overall, it can be said that relatively little is known about bimetallic nanoparticles in terms of their structure and shape.

Noble metal nanocrystals (Au, Ag) have attracted significant scientific attention in nano-optics due to their unique characteristics of localized surface plasmon resonance, demonstrating LSPR bands in the visible spectrum region. Moreover, their extinction coefficient has proven to be at least three to four orders of magnitude higher than that of any organic molecule. Consequently, these nanomaterials represent attractive transducers, for example, for the development of colorimetric biosensors [9].

Currently, gold nanoparticles (Au NP) have become the most widespread due to their well-established synthesis, high chemical stability, and biocompatibility. However, compared to Au NP, silver nanoparticles (Ag NP) of the same size have a much higher extinction coefficient, and their use can thus significantly improve nanoparticle sensitivity. Until now, the enormous potential of silver nanoparticles has been underutilized, mainly due to easy chemical decomposition through oxidation and poor colloidal stability in the absence of organic coating [10]. However, these coatings are not suitable for sensing applications as they isolate the metallic core from the environment, preventing the LSPR band shift typically used for analyte detection. Therefore, one solution to this problem could be the formation of binary nanoparticles of Ag–Au, which are expected to possess greater chemical stability due to the presence of gold atoms on the surface.

Note that the magnitude of localized surface plasmon resonance is influenced by multiple factors. First and foremost is size. Thus, as the average particle size in an array increases, the maximum LSPR peak position shifts toward longer wavelengths [11]. But the nanoparticle material affects the LSPR maximum position even more significantly. Changing the average particle diameter from $D = 7$ nm to $D = 60$ nm allows varying the LSPR maximum position within a range of about 50 nm. However, with a gradual change in the composition of Ag–Au alloy nanoparticles from Ag to Au, it can be varied within about 120 nm [1]. Theoretical modeling [12] shows that λ_{max} in the absorption spectra of spherical nanoparticles of Ag–Au depends almost linearly on their composition, i.e., on the molar ratio of metals in the particle.

Thus, binary gold and silver alloy nanoparticles are of great practical interest due to the possibility of tuning the spectral position and amplitude of LSPR by changing the composition, size, shape, structure, and dielectric environment of nanoparticles. Adjustment of the target chemical composition of the nanoalloy opens an additional way to control optoelectronic properties and can also improve practically important characteristics of nanoparticles. Since the Ag–Au system represents a series of continuous solid solutions, it becomes possible to smoothly change the position of the LSPR maximum in the wavelength range corresponding to pure Ag and pure Au by selecting the percentage ratio of components [2].

In addition, the quality and type of nanoparticle structure play a huge role in plasmonic effects. Achieving specific particle morphology depends exclusively on the correct combination of precursors, as well as appropriate temperature selection [13]. Thus, the aim of this work was to investigate through computer modeling the processes of internal structure formation of binary alloy nanoparticles of Ag–Au depending on their target composition, size, and level of thermal exposure during the simulation of certain physical synthesis methods.

2. COMPUTER MODEL

For a physically correct solution of the given task, it is necessary, first of all, to determine the research methodology. Undoubtedly, the results of real experiments are precisely the factor that allows us to verify our assumptions and hypotheses. However, in the case of analyzing the thermal evolution of small nanoparticles (nanoclusters), not everything is so straightforward. Ultimately, it was experimentally observed that the internal ordering of nanoparticles, even at room temperature, is a very complex process dependent on particle size and environmental properties.

In our opinion, computer modeling can be the most suitable way to obtain the information we are interested in. This methodology allows varying a wide range of both internal and external parameters of nanoclusters (size, shape, initial structure, temperature, rate of thermal energy input/output, etc.) within broad limits, which gives us extensive scope for possible model experiments, often unattainable in real experiments. The molecular dynamics (MD) method was chosen as the basis for modeling, which is quite adequate in terms of determining the structures of metallic nanoparticles with the size we are interested in.

Another important aspect of modeling real systems is choosing the correct form of interatomic interaction. As practice has shown, the application of the EAM potential (embedded atom method) in simulating small metallic nanoparticles cannot be considered particularly successful due to the basic features of constructing this type of interaction. In the case of sufficiently large particles, this method can provide adequate results, but when analyzing the small nanoclusters we study, the data obtained based on it cease to be physically correct.

Therefore, in the presented work, computer modeling of nanoparticles Ag–Au was conducted using the modified tight-binding potential TB-SMA [14], which has proven itself well in studying the internal structure of nanoclusters of various chemical elements. The method is based on the fact that a large group of properties of transition metals can be completely determined from the density of states of external *d*-electrons. The second moment of the density of states is μ_2 and it has been experimentally established that the cohesion energy of metals is proportional to the width of the density of states, which in the second moment approximation is simply $\sqrt{\mu_2}$. If only *dd*σ-, *dd*π- and *dd*δ-orbitals are taken into account, then, according to this model, the band energy of atom *i* can be written as a function

$$E_B^i = -\left(\sum_j \xi_{\alpha\beta}^2 e^{-2q_{\alpha\beta}\left(r_{ij}/r_0^{\alpha\beta}-1\right)}\right)^{1/2}, \qquad (1)$$

which depends only on the distance between atoms *i* and *j*, i.e. r_{ij}, and formally represents the same as the embedding function in the embedded atom method. Additionally, the model includes a term responsible for repulsive interaction in the form of a sum of Born–Mayer pair ionic potentials:

$$E_R^i = \sum_j A_{\alpha\beta} e^{-p_{\alpha\beta}\left(r_{ij}/r_0^{\alpha\beta}-1\right)}, \qquad (2)$$

where α and β are different types of atoms. Thus, the total system energy takes the form

$$E_C = \sum_j \left(E_R^i + E_B^i\right). \qquad (3)$$

The values of $\xi_{\alpha\beta}$, $p_{\alpha\beta}$, $A_{\alpha\beta}$, $q_{\alpha\beta}$ and $r_0^{\alpha\beta}$, as well as the potential cutoff radius r_c, determine the parameters of system elements and are taken directly from work [14]. The values $\xi_{\alpha\beta}$, $p_{\alpha\beta}$, $A_{\alpha\beta}$ and $q_{\alpha\beta}$ are found by fitting to experimental values of cohesion energy, lattice parameter, bulk modulus *B* and elastic constants C_{44} and C'.

The potentials developed in [14] have proven themselves very well in modeling systems in crystalline state and have undergone detailed successful verification across many indicators. In particular, comparisons were made with experimental data for various parameters of point defects (vacancies, interstitials, and their small complexes), several thermodynamic properties of metals (melting temperature, transition heat, heat capacity, thermal expansion coefficient, Gruneisen constant, etc.), as well as phonon spectra. It should be noted that the characteristics calculated in [14] differ from experimental results by no more than 3–5%.

The system temperature was determined through the average kinetic energy of atoms, calculated using the Verlet velocity algorithm [15] with a time step of 1.0 fs. As initial objects, spherical clusters were used, obtained by cutting from an ideal Ag crystal lattice, in which some silver atoms were randomly replaced with gold atoms in our target percentage ratio.

Another important aspect of modeling is the system's interaction with the heat reservoir. For the molecular dynamics method, the microcanonical (NVE) ensemble is natural, for which energy is a constant value. For such purposes, a whole series of special techniques has been proposed and developed, particularly the Andersen thermostat, which we used in our calculations.

This thermostat is used to simulate the process of gradual temperature change at a given rate. To solve this problem, Ag–Au NP atoms xperience random collisions with certain virtual objects simulating atoms of cold inert gas. The effect of collisions manifests in the fact that the velocity of Ag–Au NP decreases randomly compared to the Maxwell-Boltzmann distribution at the previous temperature. In our case, the cooling rate of the atoms of the metal under consideration is controlled by the frequency of their collisions with atoms of the heat reservoir. Then, based on the Andersen thermostat, a procedure for gradual cooling of Ag–Au NPs to room temperature was carried out with three different rates of thermal energy removal. The range of simulated thermal impact rates was from $0.25 \cdot 10^{12}$ K/s to $1.25 \cdot 10^{12}$ K/s, which corresponded to simulation times of 2.5 ns and 0.5 ns, respectively. This range of rates is typical for the problems considered in this work, which is confirmed, for example, by research [16].

The simulation was performed using the MDNTP computer program developed by Dr. Ralf Meyer, University Duisburg Germany. Then, using OVITO and XMakemol visualizers, the actual appearance and structure of the studied nanoparticles were determined.

3. RESULTS AND DISCUSSION

In the last few decades, a large number of studies have been devoted to the controlled synthesis of noble metal nanoparticles with uniform morphology and size. Thus, the following production methods were significantly developed: solvothermal [17–19], electrochemical [20, 21] and photochemical [22], allowing to obtain metallic NPs with various regular internal structures. For example, Mirkin et al. performed the transformation of silver nanocrystals from spherical to icosahedral [23]. Yang et al. successfully obtained branched gold nanocrystals with tunable localized surface plasmon resonance (LSPR) characteristics and used the obtained Au NPs as a substrate for quantitative determination of heme concentration in human erythrocyte cytosol [24]. The structure of the synthesized nanoparticles was studied using transmission electron microscopy (TEM), extended X-ray absorption fine structure spectroscopy (EXAFS), and X-ray diffraction.

When considering the preparation of SERS substrates, there are two main approaches. The first is the most precise and involves the use of photolithography methods. It allows the formation of highly ordered nano-objects positioned on the surface with specified uniform NP sizes and defined distances between them. Naturally, such structures have a high SERS effect and the best reproducibility of measurement results. The only disadvantage of such SERS substrates is the high labor intensity of manufacturing and inevitably high cost. The second approach involves the formation of nanoparticles from solutions by chemical methods, which is the simplest and cheapest way. This method allows for fairly good control of particle size, however, the transfer of these particles onto a solid surface with the formation of an ordered array is poorly reproducible. Often, nanoparticles uncontrollably accumulate into agglomerates chaotically, which makes it impossible to reproduce measurement results on such surfaces [1].

However, ordered arrays of NPs on SERS substrates can also be formed by physical method of thermal evaporation in vacuum. Particles in such arrays have different diameters, but their distribution is Gaussian, while the average particle size is well controlled and reproducible [1, 2], as well as the distance between them. This method occupies an intermediate position compared to the two methods mentioned above. It is significantly cheaper and less labor-intensive compared to the lithographic method, more precise and reproducible than the chemical method.

Since this particular variant of SERS substrate preparation was chosen to model formation processes of binary Ag–Au nanoparticles [1, 2], let's examine it in more detail. The initial condensate of Ag and Au atoms was obtained by evaporating silver and gold samples, and the particles formed from the gas phase were then deposited on an inert surface. The atoms evaporated into vacuum from a point source maintained high temperature, as their movement trajectories are divergent, and the concentration of atoms in vacuum is low. All this

makes energy exchange between them unlikely [2]. The combination of atoms into dimers also leads to a sharp increase in kinetic energy in the system, which results in a similar sharp rise in temperature. That is, when two separate atoms collide forming a stable bond between them, part of the bond energy transforms into kinetic degrees of freedom, which causes the temperature to rise [25, 26]. For this reason, during condensation by method [1, 2], we are actually dealing with the impact of a hot flow of nanoparticles on the deposition surface. This aspect of synthesis appears quite important to us, as binary Ag–Au nanoparticles are applied to the substrate in a disordered, amorphous state.

As shown in [2], the initial condensate in this case was an array of small separately located particles of rather complex non-spherical shape. Subsequently, the obtained samples were annealed in vacuum at a residual pressure of $1 \cdot 10^{-5}$ Torr for 60 minutes, which led to the transformation of the array of particles with arbitrary appearance into an array of NPs with shape close to spherical [2], which was then cooled to room temperature. Similar results were recorded in other experiments [27, 28].

For computer simulation of the above processes, we created three primary arrays of Ag–Au NP with ideal FCC structure with a diameter of 2.0, 4.0 and 6.0 nm of various target compositions from $Ag_{90}Au_{10}$ to $Ag_{50}Au_{50}$. Then the nanoparticles of the binary compound Ag–Au were heated to completely destroy their long-range order to temperatures $T = 1500$ K, which excluded the presence of residual crystal phase nuclei in the NPs. After the formation process of the Ag–Au NP array with primary amorphous structure, it was subjected to a smooth cooling procedure with controlled rate of thermal energy removal to a temperature of 300 K.

The conducted modeling showed that even with a minor addition of gold impurity to the Ag cluster, the result can differ quite significantly from the case of chemically pure metal. Let's first present our data for Ag NPs subjected to exactly the same computer simulation [29]. Here, we studied the dependence of the percentage ratio of amorphous and crystalline structures appearance on cluster size and heat removal rate from the model system. Analysis of results obtained during cooling of silver nanoclusters of various diameters from molten state showed that there is a clear dependence of crystalline or amorphous structure formation process on thermal energy removal rate. Let's limit ourselves here to considering only two extreme simulated cooling rates. At a low rate of thermal energy removal, corresponding to a cooling time of $\tau = 2.0–2.5$ ns, all Ag NP ($D = 2.0–10.0$ nm) had clearly expressed crystalline structure (Ih, Dh, FCC/HCP). When reducing the cooling time to 0.5 ns, a significant decrease in the percentage of crystalline modifications occurrence was observed. Thus, at Ag NP diameter of $D = 2.0$ nm, approximately 30% nanoparticles had amorphous structure, at $D = 4.0$ nm – already about 40%, and NPs with $D = 6.0$ nm showed a surge in probability of amorphous structures appearance to 80%–90%. However, even at such a high rate of thermal energy removal, only at cluster diameter of $D = 10.0$ nm did all studied clusters consistently possess disordered structure.

Tables 1–3 present the results of modeling conducted for binary Ag–Au particles with diameters of 2.0, 4.0 and 6.0 nm respectively.

Table 1. Results of modeling the crystallization process of nanoclusters Ag–Au of different target compositions with a diameter of 2.0 nm depending on cooling time. Structure fixation percentages are given with rounding

Target composition	$Ag_{50}Au_{50}$			$Ag_{60}Au_{40}$			$Ag_{70}Au_{30}$			$Ag_{80}Au_{20}$			$Ag_{90}Au_{10}$		
Cooling time, ns	0.5	1.5	2.5	0.5	1.5	2.5	0.5	1.5	2.5	0.5	1.5	2.5	0.5	1.5	2.5
Proportion of amorphous clusters, %	90	70	70	100	70	60	100	90	70	70	90	40	50	50	10
Proportion of crystalline clusters, %															
Ih	10	-	10	-	10	30	-	-	20	10	10	50	40	30	80
Dh	-	20	20	-	-	10	-	10	-	20	-	-	10	10	
FCC/HCP	-	10	-	-	20	-	-	-	10	-	-	10	-	10	10

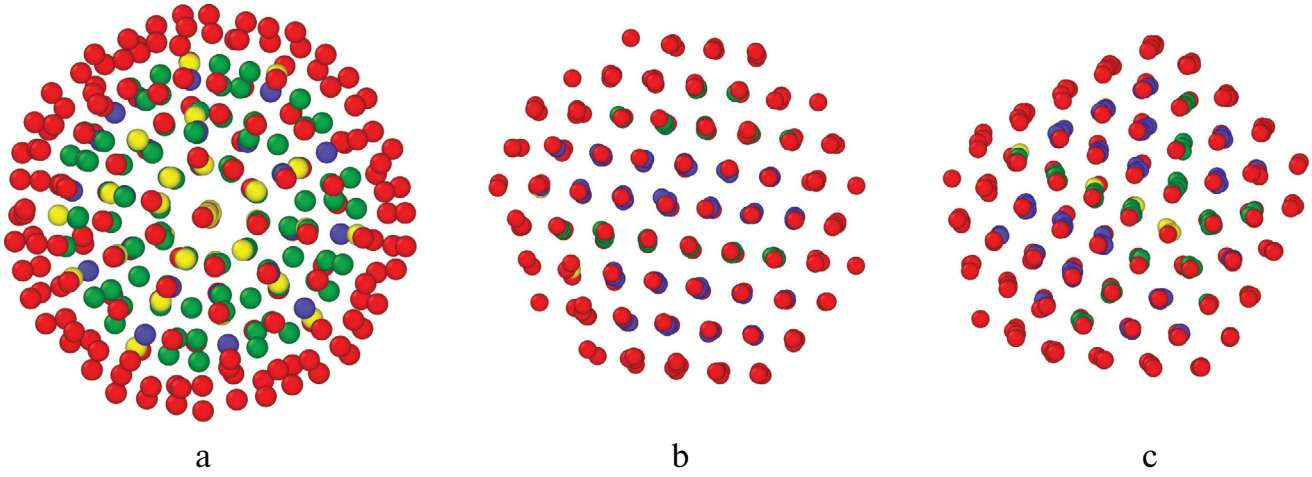

Fig. 1. (In color online) Examples of crystalline structures of Ag_{90}–Au_{10} nanoclusters with 2.0 nm diameter, obtained during cooling from melt: Ih (a), FCC/HCP (b), Dh (c) (Different colors of silver atoms are determined by standard CNA-methodology (common neighbors analyze), analyzing the number of bonds of each atom in the first, second and third coordination spheres. Thus, a red atom indicates that its coordination number in the first sphere is less than 12, while a yellow atom indicates that its coordination number in the first sphere equals 12, but in the second is less than the value characteristic for close-packed structures (FCC, HCP). Blue atoms show that their coordination numbers in the first, second and third coordination spheres correspond to FCC structure, and green corresponds to HCP

It can be seen that the addition of gold atoms to Ag NP at melt cooling time $\tau = 2.5$ns only affected the smallest Ag–Au NPs with diameter $D = 2.0$ nm, where with increasing percentage of gold atoms, a similar increase in the probability of amorphous phase appearance was observed, reaching its maximum value at 60–70%. At $D = 4.0$ and 6.0 nm, similar to Ag NP, the amorphous phase at this rate of thermal energy removal was not detected, despite the fact that the target composition changed to its maximum value $Ag_{50}Au_{50}$.

At a cooling time of $\tau = 0.5$ ns, the effect of adding a second chemical element proved to be more significant. Thus, in the case of Ag NPs with $D = 2.0$ nm, the amorphous phase was observed in 30%, and for binary nanoparticle Ag–Au in 50–100% model experiments, gradually increasing the probability of its appearance with the increase in the percentage of gold atoms. With increasing size of Ag–Au NPs the tendency persisted, but with an increase in the minimum percentage of amorphous phase fixation. That is, at such a high rate of heat energy removal, the addition of gold atoms to Ag NPs led to an almost linear increase in the probability of amorphous structure appearance.

Let's try to explain the obtained result. For this, we will analyze the behavior of Au NPs under the same conditions of the computer experiment [30]. As expected, the process of Au NP structure formation also strongly depended on the cooling rate. The main trend was an increase in the percentage of amorphous structures with increasing cooling rate.

Moreover, while for clusters with diameters up to 2.4 nm this percentage was relatively low ($\approx$ 10%), for particles of size 2.5–3.4 nm it already fluctuated in the range from 40% to 60%, and for larger clusters ($D = 4$–5 nm) increased to $\approx$ 80% ($\tau = 0.5$ ns).

This result is primarily explained by the fact that systems with a larger number of atoms do not have enough time to form a specific crystalline structure, which leads to such a high percentage of disordered particle fixation.

Thus, it can be concluded that the incorporation of gold atoms into Ag NPs has a clear destabilizing effect on the formation of an ordered internal structure in the binary Ag–Au nanoparticle [31, 32]. However, since atomic restructuring here has a diffusion character strongly dependent on temperature, in the case of our simulation of binary Ag–Au particle crystallization from melt, the cooling time may not be sufficient to complete this process, which results in the "freezing" of the amorphous phase. It is also obvious that the higher the percentage of gold atoms, the more likely the disordered state will be, at least at a high rate of thermal energy removal. Consequently, for Ag–Au NPs on the SERS substrate to be in an ordered crystallographic state at any target composition, it is necessary to use nanoparticles with a diameter of $D > 2$–3 nm and achieve slow cooling of the system.

Table 2. Results of cooling simulation for Ag–Au nanoparticles from melt of various target compositions with 4.0 nm diameter depending on cooling time. Structure fixation percentages are given with rounding

Target composition	$Ag_{50}Au_{50}$			$Ag_{60}Au_{40}$			$Ag_{70}Au_{30}$			$Ag_{80}Au_{20}$			$Ag_{90}Au_{10}$		
Cooling time, ns	0.5	1.5	2.5	0.5	1.5	2.5	0.5	1.5	2.5	0.5	1.5	2.5	0.5	1.5	2.5
Amorphous clusters, %	100	80	–	100	100	–	90	80	–	80	50	–	60	10	–
Crystalline structures, %															
Ih	–	–	30	–	–	30	–	–	20	–	–	20	10	10	40
Dh	–	10	30	–	–	20	–	–	20	–	20	50	–	30	50
FCC/HCP	–	10	40	–	–	50	10	20	60	20	30	30	30	50	10

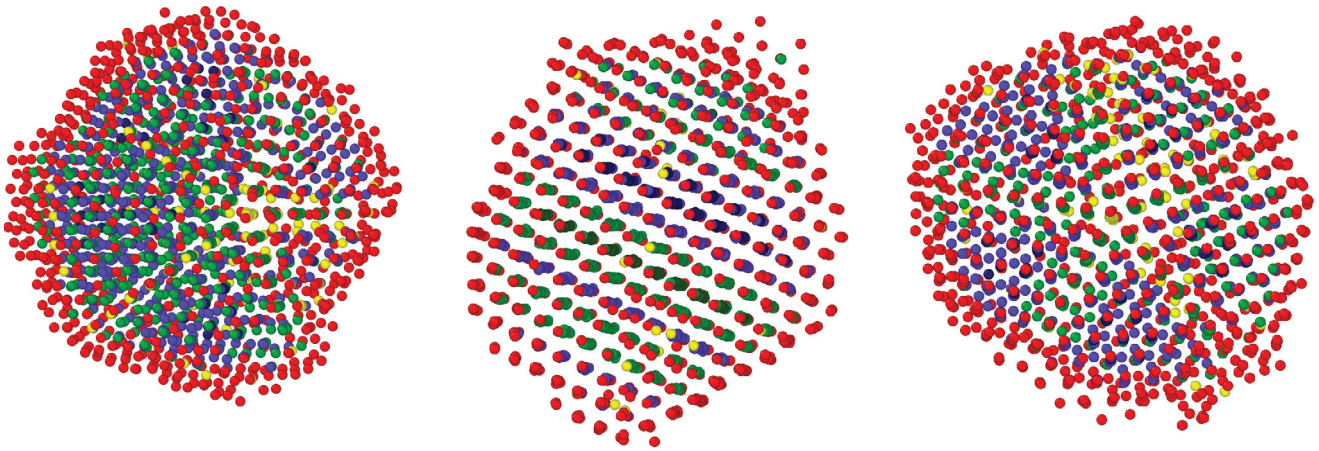

Fig. 2. (In color online) Examples of crystalline structures of nanoclusters $Ag_{50}Au_{50}$ with 4.0 nm diameter, obtained during cooling from melt: Ih (a), FCC/HCP (b), Dh (c). Different colors of silver atoms are determined by standard CNA methodology, analyzing the number of bonds of each atom in the first, second, and third coordination spheres. Thus, a red atom indicates that its coordination number in the first sphere is less than 12, a yellow atom indicates that its coordination number in the first sphere equals 12, but in the second sphere is less than the value characteristic for close-packed structures (FCC, HCP). Blue atoms show that their coordination numbers in the first, second, and third coordination spheres correspond to FCC structure, while green atoms correspond to the HCP

The first condition can be met by adjusting the vacuum-thermal evaporation process of precursors itself, changing the distance from the crucible to the target and the evaporation rates of Ag and Au suspensions, and the second by using a substrate heated during crystallization of Ag–Au NPs.

Let us now turn to the question of determining the specific type of crystal structure of binary Ag–Au NPs, obtained through our MD simulation. To explain the importance of such information, we present the following reasoning. Without the formation of a strong dipole, light scattering and absorption by nanoparticles will be insignificant. For highly symmetric figures, such as spheres, cubes, and octahedra, a strong dipole can be easily formed. Charge separation at the corners of a cube will create a dipole because the corners are on opposite sides of the symmetry line. Similarly, for spheres, charge separation occurs in a completely isotropic medium [33]. However, nanostructures lacking such symmetry, for example triangular plates, cannot form a strong dipole, resulting in weak light absorption. Therefore, the internal structure and shape of NPs, besides their size, can become one of the determining factors for stability and magnitude of the plasmon effect. To confirm these statements, we present the following experimental data for Ag NPs [34], which is our basic chemical element: the main resonance peak for a spherical NP is recorded in the range of 320–450 nm, for cubic 400–480 nm, for decahedron the resonance occurs at 350–450 nm, and for octahedron at 400–500 nm.

Analysis of the internal structure of nanoclusters shows (Table 1) that the preferred crystal structure

Table 3. Results of cooling simulation of Ag–Au nanoparticles from melt of various target compositions with a diameter of 6.0 nm depending on the cooling rate. Structure fixation percentages are given with rounding

Target composition	$Ag_{50}Au_{50}$			$Ag_{60}Au_{40}$			$Ag_{70}Au_{30}$			$Ag_{80}Au_{20}$			$Ag_{90}Au_{10}$		
Cooling time, ns	0.5	1.5	2.5	0.5	1.5	2.5	0.5	1.5	2.5	0.5	1.5	2.5	0.5	1.5	2.5
Amorphous clusters, %	100	90	–	100	70	–	100	100	–	100	50	–	70	10	–
Crystalline structures, %															
Ih	–	–	10	–	–	–	–	–	10	–	–	10	–	–	10
Dh	–	–	20	–	–	10	–	–	–	–	–	10	–	–	10
FCC/HCP	–	10	70	–	30	90	–	–	90	–	50	80	30	90	80

for the diameter $D = 2.0$ nm is the Ih-configuration, in some cases competing with the Dh-modification, while FCC/HCP morphology (Fig. 1) occurs noticeably less frequently. The stabilization of the Ih-phase can be explained by the alloying of elements with different atomic (ionic) sizes, as this mismatch can compensate for the existing deformation in icosahedral shells due to the increasing difference between atomic distances along radial and tangential directions. Thus, from a theoretical perspective, an ideal Ih-cluster of binary alloy Ag–Au should possess an Ag-enriched core and a surface with predominant placement of gold atoms. This agrees with the fact that the icosahedron core experiences compression, making it energetically more favorable for smaller Ag atoms (ions) to be located there, while the NP Ih surface experiences stretching, making the placement of small atoms there impractical.

However, this is only valid for a certain size of binary nanoparticle, approximately up to a diameter of $D = 2.0$–3.0 nm, even for alloys with large differences in atomic sizes [35]. Beyond this size, the probability of icosahedral phase appearance begins to decrease noticeably. The reason lies in the general energetic instability of the atomic structure mentioned above. Thus, even in the case of Au NPs [30], data analysis showed that for clusters with diameters not exceeding 3.0 nm, the probability of icosahedral phase appearance prevails over others, constituting 50–60%, and is practically independent of cooling rate. At larger cluster sizes, the probability of icosahedral morphology appearance generally decreases, but the following trend is quite evident: as the cooling rate decreases, the proportion of clusters with icosahedral structure increases quite uniformly.

Looking in more detail at the nature of crystalline structures obtained during simulation, one can see confirmation of the pattern we found earlier. Thus, for nanoclusters Ag–Au with a diameter of $D = 4.0$ nm, the presence of Ih-phase is characteristic specifically at maximum crystallization time of $\tau = 2.5$ ns or for particles with low gold content (target composition $Ag_{90}Au_{10}$). Under other conditions, icosahedral structure was not observed during MD experiments (Table 2). Thus, it can be concluded that the considered diameter of binary Ag–Au NP, apparently, lies in the size range where, under conditions of smooth crystallization with high speed, the icosahedral structure ceases to be the most stable and is replaced by Dh- or FCC structure. In work [36], a set of 923, 1415, 3871, 10179 atomic gold clusters of three different structures (icosahedral, defective icosahedral, and amorphous), obtained from melt crystallization at different rates, was analyzed, and it was concluded that from an energetic perspective, the defective icosahedral configuration is the most stable, which can be seen in Fig. 2.

Regarding the probability of total occurrence of Ag–Au NPs with five-fold symmetry (Ih + Dh) it was maximum at the target composition $Ag_{90}Au_{10}$ ($\approx$90%), ultimately decreasing to 50–60% for compositions with the highest gold atom content $Ag_{60}Au_{40}$ and $Ag_{50}Au_{50}$. Accordingly, with increasing Au atom content, we observed a gradual increase in FCC/HCP phase from 10% to 50–60%, which was merely a consequence of reduced probability to encounter a binary Ag–Au NP specifically with five-fold structure due to the growth of internal stresses arising in this case, the reason for which was indicated above.

When considering the behavior of nanoparticles Ag–Au with increasing cooling rate, there was a significant increase in finding them in amorphous state, just as with Au NPs [30]. At $\tau = 0.5$ ns, the percentage of fixation of this polytypic modification was 60–100%, increasing with the growing percentage of gold atoms, which once again proves its destabilizing effect during the formation of ordered structure of binary nanoparticles Ag–Au. Thus, for pure silver under the same crystallization conditions, the amorphous phase was recorded in 40% experiments, at the target composition $Ag_{90}Au_{10}$ already in 50%, at composition $Ag_{80}Au_{20}$ in 70%, and at the target composition $Ag_{70}Au_{30}$ and above in practically 90–100% experiments.

Let's proceed by considering the MD simulation results obtained for an ensemble of binary Ag–Au NPs with a diameter of $D = 6.0$ nm (Table 3). It can be seen that at this size, the amorphous phase is not detected only at the maximum cooling time of $\tau = 2.5$ ns; at a higher heat removal rate ($\tau = 0.5$ and 1.5 ns), it is observed in 100% cases, starting from composition. For this array, with an increase in the percentage of gold atoms in Ag–Au NPs there is a similar increase in the probability of disordered structure. That is, there is a clear tendency that an increase in the average size of NPs in the array and/or an increase in the percentage of gold atoms in the binary Ag–Au NPs leads to an increase in the probability of amorphous structure formation in NPs, and such growth often has an almost linear character. Also, the rate of thermal energy removal has a determining influence on the process of internal structure formation. Thus, even for such relatively large particles ($D = 6.0$ nm) at a cooling time of $\tau = 2.5$ ns, the amorphous phase is not detected at all, while at $\tau = 1.5$ ns it is observed in almost 100%.

Thus, based on the simulation results, several main conclusions can be drawn. First, the introduction of gold atoms into a silver nanocluster has a destabilizing effect on the processes of internal structure ordering. Second, with an increase in the percentage of gold atoms in the binary nanoparticle Ag–Au there is an increase in the probability of amorphous structure formation, and such growth often has an almost linear character. Third, in small nanoclusters Ag–Au with a diameter less than $D < 2$–3 nm, it is very difficult to achieve strictly crystalline structure formation at any target composition. Fourth, the average size of the nanoparticle array Ag–Au of 4.0 nm is the most suitable for the formation of close-packed structures at a relatively low rate of thermal energy removal. Fifth, with increasing average size, the probability of forming five-fold symmetry in binary particles Ag–Au significantly decreases.

4. CONCLUSION

It is well known that gold and silver are mutually soluble in each other in any proportions, forming a continuous series of solid solutions. The dissolution of impurities in metal (Au in Ag or Ag in Au) locally deforms the crystal lattice and causes a disruption of periodicity, which in the case of nanoscale can lead to various types of external form and internal structure of NPs. These processes can lead to a reduction in the electron mean free path and, consequently, to an increase in its scattering frequency, which affects the intensity of the SERS effect compared to pure elements. However, at the same time, binary nanoparticles Ag–Au provide the possibility of tuning the spectral position and amplitude of LSPR by changing the target composition, size, shape, and structure.

Thus, the transmission spectra obtained in work [2] demonstrated the presence of a SERS peak for Ag NPs at approximately 440 nm wavelength, for Au NPs at approximately 580 nm wavelength, and for Ag–Au NPs at approximately 550 nm wavelength. The transformation of arrays as a result of annealing led to a shift of SERS wavelengths of all three samples to the short-wavelength region of the spectrum and a slight increase in integral transmission, namely: the SERS wavelength for the Ag NP array (with predominant particle size of approximately 8 nm) was approximately 420 nm, for Au NPs (with predominant size of approximately 7 nm) approximately 520 nm, and for Ag–Au particle array (with predominant size of approximately 10 nm) – approximately 490 nm. Such a shift in minimum positions for annealed samples was associated with changes in nanoparticle shape, particularly with nanoparticles acquiring spherical shape [2], as well as a decrease in their geometric cross-section, which, in turn, led to narrowing of resonances.

That is, the high sensitivity of surface plasmon resonance to the shape of nanoparticles is well confirmed experimentally. In [37], a study was

conducted on the effect of Au nanorods and Au nanospheres on the SERS effect, and it turned out that the plasmon radiation of Au nanorods and nanospheres differs quite significantly, being 650 and 520 nm respectively. In addition to the nanorods and nanospheres considered in [37], other plasmonic nanostructures such as nanocubes and nanostars were experimentally analyzed. It turned out that due to their sharp edges and corners, these structures tend to maximize the enhancement of the main properties of the plasmon effect. In general, structures with sharp angles have peaks shifted to the red region compared to rounded structures of similar sizes. However, truncation of angles affects not only the radiation frequency but also changes the electric field near the particle surface, leading to light concentration in nanoscale volumes and sharp increase in luminescence intensity in these regions.

The formation of icosahedral structure of nanoparticles in this context is of fundamental importance. It is clear that the greatest volume minimization is determined by the formation of Mackay icosahedron (Ih), whose surface consists of 20 equilateral triangles. Larger Mackay icosahedra are formed by adding further Ih-shells, which leads to minimization of cluster surface area and, consequently, gain in surface energy. Thus, by forming a regular icosahedral (decahedral) structure in Ag–Au nanoparticles, we solve the task of forming a highly symmetric figure necessary for increasing the luminosity of the SERS substrate.

FUNDING

The study was carried out with the grant from the Russian Science Foundation No. 23-12-20003, https://rscf.ru/project/23-12-20003/, with parity financial support from the Government of the Republic of Khakassia.

REFERENCES

1. D. G. Gromov, S. V. Dubkov, A. I. Savitskiy, Yu. P. Shaman, A. A. Polokhin, I. A. Belogorokhov, and A. Yu. Trifonov, App. Surf. Sci. 489, 701 (2019).

2. D. G. Gromov, I. V. Melnikov, A. I. Savitskiy, A. Yu. Trifonov, E. N. Redichev, V. A. Astapenko, Tech. Phys. Lett. 43, 3 (2017).

3. Z. Ciplak, C. Gokalp, B. Getiren, A. Yildiz, and N. Yildiz, Green Process Synth. 7, 433 (2018).

4. P. C. Lee and D. Meisel, J. Phys. Chem. 86, 3391 (1982).

5. M. Khan, Kh. Al-hamoud, Z. Liaqat, M. R. Shaik, S. F. Adil, M. Kuniyil, H. Z. Alkhathlan, A. AlWarthan, M. Rafiq H. Siddiqui, M. Mondeshki, W. Tremel, M. Khan, and M. N. Tahir, Nanomaterials 10, 1885 (2020).

6. Th. J. A. Slater, A. Macedo, S. L. M. Schroeder, M. G. Burke, P. O'Brien, P. H. C. Camargo, and S. J. Haigh, Nano Lett. 14, 1921 (2014).

7. Y. Qin, B. Wang, Y. Wu, J. Wang, X. Zong, and W. Yao, Crystals 11, 769 (2021).

8. J. Haug, M. Dubiel, H. Kruth, and H. Hofmeister, J. Phys.: Conf. Ser. 190, 012124 (2009).

9. M. Retout, I. Jabin, and G. Bruylants, ACS Omega 6, 19675 (2021).

10. V. I. Kukushkin, A. B. Vankov, I. V. Kukushkin, JETP Letters 98, 72 (2013).

11. P. Zhang, Y. Li, D. Wang, and H. Xia, Part. Part. Syst. Charact. 33, 924 (2016).

12. J. Zhu, Phys.E: Low-Dimens. Syst. Nanostruct. 27, 296 (2005).

13. M. Ramos, D. A. Ferrer, R. R. Chianelli, V. Correa, J. Serrano-Matos, and S. Flores, J. Nanomaterials 2011, 374096 (2011).

14. A. Rapallo, G. Rossi, R. Ferrando, A. Fortunelli, B. C. Curley, L. D. Lloyd, and R. L. Johnston, J. Chem. Phys. 122, 194308 (2005).

15. L. Verlet, Phys Rev. 159, 98 (1967).

16. S. H. Lee, S. S. Han, J. K. Kang, J. H. Ryu, and H. M. Lee, Surf. Sci. 602, 1433 (2008).

17. Y. Qin, W.F. Pan, D.D. Yu, Y.X. Lu, W.H. Wu, and J.G. Zhou, Chem. Commun. 54, 3411 (2018).

18. Y.Z. Qin, Y.X. Lu, D.D. Yu, and J.G. Zhou, Cryst. Eng. Comm. 21, 5602 (2019).

19. L. Litti, J. Reguera, and F. Abajo, Nanoscale Horiz. 5, 102 (2020).

20. N. Tian, Z. Y. Zhou, N. F. Yu, L. Y. Wang, and S. G. Sun, J. Amer. Chem. Soc. 132, 7580 (2010).

21. J. H. Du, T. Sheng, C. Xiao, N. Tian, J. Xiao, A. Xie, S. Liu, Z. Zhou, and S. G. Sun, Chem. Commun. 22, 3236 (2017).

22. G. R. Guillerm, D. N. Pablo, R. Antonio, P. Alejandro, T. Gloria, G. Jesus, B. Luis, L. Pablo, G. M. Luis, A. P. Mauricio et al., Science 358, 640 (2017).

23. M. R. Langille, J. Zhang, M. L. Personick, S. Li, and C. A. Mirkin, Science 337, 954 (2012).

24. Z. Cai, Y. Hu, Y. Sun, Q. Gu, P. Wu, C. Cai, and Z. Yan, Anal. Chem. 93, 1025 (2021).

25. S. L. Gafner, Yu. Ya. Gafner, JETP 134, 831 (2008).

26. Y. Ya. Gafner, S. L. Gafner, D. A. Ryzkova, and A. V. Nomoev, Beilstein J. Nanotechnology 12, 72 (2021).

27. G. P. Shevchenko, V. A. Zhuravkov, and G. V. Shishko, SN Appl. Sci. 1, 1192 (2019).

28. Y. Hu, A.-Q. Zhang, H.-J. Li, D.-J. Qian, and M. Chen, Nanoscale Research Lett. 11, 209 (2016).

29. D. A. Bashkova, Yu. Ya. Gafner, S. L. Gafner, L. V. Redel, Fundamental Problems of Modern Materials Science 15, 313 (2018).

30. Yu. Ya. Gafner, Zh. V. Golovenko, S. L. Gafner, JETP 143, 288 (2013).

31. Y. Gafner, S. Gafner, L. Redel, and I. Zamulin, J. Nanoparticle Research 20, 51 (2018).

32. Yu. Ya. Gafner, S. L. Gafner, Zh. V. Golovenko, Letters on Materials 10, 33 (2020).

33. F. J. Abajo, Rev. Mod. Phys. 79, 1267 (2007).

34. M. Rycenga, C. M. Cobley, J. Zeng, W. Li, Ch. H. Moran, Q. Zhang, D. Qin, and Y. Xia, Chem. Rev. 111, 3669 (2011).

35. L. R. Owen, H. Y. Playford, H. J. Stone, and M. G. Tucker, Acta Materialia 125, 15 (2017).

36. Y. H. Chui, G. Grochola, I. K. Snook, and S. P. Russo, Phys. Rev. B 75, 033404 (2007).

37. T. Tanaka, Y. Totoki, A. Fujiki, N. Zettsu, Y. Miyake, M. Akai-Kasaya, A. Saito, T. Ogawa, and Y. Kuwahara, Appl. Phys. Express 4, 032105 (2011).